RESEARCH ARTICLE | AUGUST 28 2023

Couette flow at high Knudsen number between wall and liquid boundaries FREE

Kazumichi Kobayashi ; Kota Aoki; Hirofumi Tabe ; Hiroyuki Fujii ; Toshiki Nara ; Hideyoshi Takashima ; Nobuyuki Oshima ; Masao Watanabe

Physics of Fluids 35, 082021 (2023)
https://doi.org/10.1063/5.0164544
CHORUS

Physics of Fluids ARTICLE pubs.aip.org/aip/pof

Couette flow at high Knudsen number between wall and liquid boundaries

Cite as: Phys. Fluids **35**, 082021 (2023); doi: 10.1063/5.0164544
Submitted: 23 June 2023 · Accepted: 9 August 2023 ·
Published Online: 28 August 2023

Kazumichi Kobayashi,[1,a)] Kota Aoki,[1] Hirofumi Tabe,[1] Hiroyuki Fujii,[1] Toshiki Nara,[2] Hideyoshi Takashima,[2] Nobuyuki Oshima,[1] and Masao Watanabe[1]

AFFILIATIONS

[1]Division of Mechanical and Space Engineering, Faculty of Engineering, Hokkaido University, Kita 13 Nishi 8, Kita-ku, Sapporo, Hokkaido 060-8628, Japan
[2]AIS Hokkaido Inc., Kita-ku, Kita 7 Nishi 1, Sapporo, Hokkaido 060-0807, Japan

[a)]Author to whom correspondence should be addressed: kobakazu@eng.hokudai.ac.jp

ABSTRACT

This paper presents molecular dynamics simulations of the Couette flow of a rarefied gas between the liquid and wall boundaries and, in particular, investigates the boundary conditions for the Boltzmann equation at the liquid interface. The simulation results for various Knudsen numbers show that the slip velocity decreases at the liquid boundary and increases at the smooth wall as the Knudsen number increases, indicating that the velocity profile of the rarefied Couette flow is asymmetric. One reason for this is backscattering, in which molecules are reflected in the opposite direction to the mainstream flow, owing to molecular-scale roughness at the liquid boundary. It has also been suggested that the backscattering effect decreases when the gas density increases. This can be understood using the local Knudsen numbers near the liquid boundary.

I. INTRODUCTION

The shear flow of a rarefied gas between the wall and liquid boundaries is a key factor in several multiphase flows of liquids and gases, for example, droplet impact and lubrication of liquid pipe flow.[1,2] An important dimensionless quantity, the Knudsen number, was used to determine the degree of rarefaction of the gas flow. The Knudsen number is defined as

$$\mathrm{Kn} = \frac{\lambda}{L}, \tag{1}$$

where λ is the mean free path of the gas molecules and L is the representative flow length. For $\mathrm{Kn} \to 0$, the gas flow can be described using a fluid dynamics equation. However, in the case of $\mathrm{Kn} = O(1)$, gas becomes rarefied, resulting in a non-equilibrium flow in which intermolecular collisions do not occur sufficiently and local equilibrium is not established. To address the rarefied gas flow, that is, high Knudsen number flow, the Boltzmann equation is an essential tool because the fluid dynamics equation based on local equilibrium cannot describe nonequilibrium phenomena.

When analyzing such rarefied gas flows using Boltzmann equation, boundary conditions at the walls and liquid boundaries are required. The boundary condition, called as the kinetic boundary condition (KBC), dictates the interactions among the wall, liquid, and gas molecules. Generally, diffuse reflection, which implies isotropic scattering, was used as the boundary condition to solve the shear flow problem.[2]

Many studies have investigated the molecular interactions between walls and gas molecules based on molecular dynamics (MD) simulations. For example, Yamamoto *et al.* investigated molecular reflection at the boundary using MD simulation and applied its results to the DSMC (direct simulation Monte-Calro) simulation of the Boltzmann equation to solve the Couette flow of rarefied gas to investigate the accommodation coefficients of the momentum, translational, and rotational energies.[3,4] Yamaguchi *et al.* investigated the energy accommodation and tangential accommodation coefficients by changing the mass or size of the gas molecules based on MD simulations.[5]

When the representative length L becomes sufficiently smaller, for example, at the nanoscale, the area affected by intermolecular potential of the boundary molecules cannot be ignored near the boundary (Fig. 1). In this case, we must determine the positions to impose KBCs at the boundaries and determine the velocity distribution function of the KBC at the boundaries.

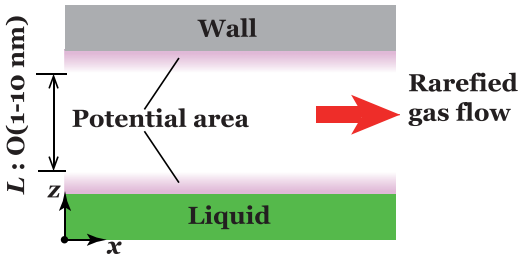

FIG. 1. Schematic of rarefied gas flow between wall and liquid boundaries.

In a pioneering work, the boundary was a wall, and the existence of a potential area near the boundary was investigated using MD simulations for a small representative length of the flow.[6] In particular, the boundary structure of a liquid boundary is more complex than that of a wall boundary, for example, a capillary wave of the molecular scale.[7] Generally, diffuse reflection is used for the functional form of KBCs for the reflected molecules at the liquid boundary when the vapor causes weak evaporation/condensation problems with small deviations from equilibrium.[8] However, it is not known whether isotropic diffuse reflection applies to the reflections of molecules on a liquid boundary when shear flow occurs.

In this study, we performed MD simulations for a rarefied gas Couette flow between wall and liquid boundaries. In addition, the results of the MD simulations were compared with those of the Boltzmann equation. Based on the results of this study, we investigated the functional form of KBCs at liquid boundaries. In addition, the difference in the functional form of KBC was investigated by changing the liquid temperature.

II. METHOD

A. Molecular dynamics simulation

In this study, argon (Ar) molecules were used as the liquid film and ambient vapor and platinum (Pt) molecules were used as the solid walls (see Fig. 2). First, the liquid film and ambient vapor were controlled using the velocity scaling method to reach a gas–liquid two-phase equilibrium state at 85, 95, or 105 K. Subsequently, the Pt walls equilibrated at each temperature in another system were inserted into the top and bottom portions of the simulation system to obtain the initial conditions. The size of the simulation system was $L_x \times L_y \times L_z = 7.212\,50 \times 7.207\,10 \times L_z\,\mathrm{nm}^3$ or $14.4250 \times 14.4142 \times L_z\,\mathrm{nm}^3$ by varying L_z as a parameter, where L_x, L_y, and L_z denote the system lengths in x, y, and z directions, respectively. Although two different lengths in the x- and y-directions were used, no difference was confirmed between the results of the two simulations for the same L_z. Periodic boundary conditions were imposed in the x and y directions, and the liquid film was placed at the center of the z direction. The Pt wall at the top boundary was moved in the positive x direction, and the Pt wall at the bottom boundary was moved in the negative x direction at a speed of $V_w = 50$ m/s. In addition to the 50 m/s case, we also checked the 25 and 100 m/s cases and confirmed that they did not produce significant differences. The total number of Pt and Ar molecules varied from 11 800 to 57 600, according to the size of the simulation system.

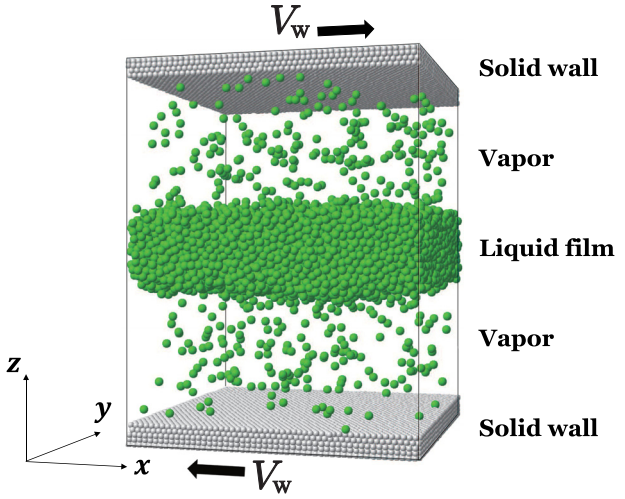

FIG. 2. Snapshot of MD simulation for rarefied gas Couette flow between wall and liquid.

In this study, the 12–6 Lennard-Jones potential, which is widely used in MD simulations, was used as the intermolecular potential of Ar:

$$\phi_{\mathrm{Ar-Ar}}(r) = 4\varepsilon_{Ar}\left[\left(\frac{\sigma_{\mathrm{Ar}}}{r}\right)^{12} - \left(\frac{\sigma_{\mathrm{Ar}}}{r}\right)^{6}\right], \tag{2}$$

where r is the intermolecular distance, molecular diameter $\sigma_{\mathrm{Ar}} = 0.3405$ nm, and energy depth $\varepsilon_{\mathrm{Ar}} = 1.654 \times 10^{-21}$ J. For the interactions between the platinum molecules, we used the first-order harmonic oscillator, which represents the interaction with only the nearest-neighbor molecules, based on previous studies,[9,10]

$$\phi_{\mathrm{Pt-Pt}}(r) = \frac{1}{2}K(r - r_0)^2, \tag{3}$$

where r_0 represents the lattice constant and K is the spring constant, with $r_0 = 0.2774$ nm and $K = 46.8$ N/m. The intermolecular potential between Ar and Pt was calculated using the following equation:

$$\phi_{\mathrm{Ar-Pt}}(r) = 4\varepsilon_{\mathrm{Ar-Pt}}\left[\left(\frac{\sigma_{\mathrm{Ar-Pt}}}{r}\right)^{12} - b\left(\frac{\sigma_{\mathrm{Ar-Pt}}}{r}\right)^{6}\right], \tag{4}$$

where

$$\sigma_{\mathrm{Ar-Pt}} = \frac{\sigma_{\mathrm{Ar}} + \sigma_{\mathrm{Pt}}}{2}, \quad \varepsilon_{\mathrm{Ar-Pt}} = a\sqrt{\varepsilon_{\mathrm{Ar}} \cdot \varepsilon_{\mathrm{Pt}}}, \tag{5}$$

where $\sigma_{\mathrm{Pt}} = 0.2475$ nm and $\varepsilon_{\mathrm{Pt}} = 8.346 \times 10^{-20}$ J. The magnitude of the intermolecular forces between Ar and Pt is variable depending on the values of a and b. In this study, $a = 0.07$ and $b = 1$ were assumed to be constant. These values of a and b were based on those used in previous MD simulations.[9,10] The cutoff distance for the intermolecular force was set to $r_c = 1.5$ nm. In these simulations, the center-of-gravity control was applied to the Ar molecules to fix the center of the liquid. The leap–frog method was used to solve the MD simulations with a time increment of 5 fs. The simulations were conducted using the in-house code.

B. Molecular gas dynamics simulation

Once the results of the MD simulation were obtained, we solved the Boltzmann equation by comparing the results of the rarefied gas flow. The ES–BGK Boltzmann equation[11] was utilized in this study to fit the Prandtl number of hard-sphere molecules as Pr = 0.66071. The ES–BGK Boltzmann equation is expressed as

$$\frac{\partial f}{\partial t} + \xi_i \frac{\partial f}{\partial x_i} = \frac{p}{\mu(1-\nu)}[G(f) - f], \tag{6}$$

where f is the velocity distribution function of gas molecules, ξ_i is the molecular velocity ($i = x, y$ or z), μ is the viscosity coefficient, p is the gas pressure, and ν is the constant value used to fit the Prandtl number, Pr,

$$\mathrm{Pr} = \frac{1}{1-\nu}. \tag{7}$$

In this simulation, the value of ν was $-1/2$. $G(f)$ can be expressed as

$$G(f) = \frac{\rho}{\sqrt{(2\pi)^3 \det(\tau_{ij})}} \exp\left(-\frac{1}{2}(\xi_i - v_i)\tau_{ij}^{-1}(\xi_j - v_j)\right), \tag{8}$$

where τ_{ij} is defined as follows:

$$\tau_{ij} = (1-\nu)RT\delta_{ij} + \nu\Theta_{ij}, \tag{9}$$

where δ_{ij} denotes the Kronecker's delta, $\rho\Theta_{ij}$ is the stress tensor, and ρ is the gas density. $R = k/m$ is the gas constant, where k is the Boltzmann constant and m is the mass of a molecule.

The finite differential method was used for the ES–BGK Boltzmann equation as a one-dimensional problem (z direction). As reported by Chu,[12] we can eliminate the molecular velocity component ξ_y by multiplying the velocity distribution function, f, by one or ξ_y^2 and integrating over the entire space of ξ_y,

$$\begin{cases} f_{xz}(z, \xi_x, \xi_z, t) = \int_{-\infty}^{\infty} f(z, \xi_x, \xi_y, \xi_z, t)\mathrm{d}\xi_y, \\ h_{xz}(z, \xi_x, \xi_z, t) = \int_{-\infty}^{\infty} \xi_y^2 f(z, \xi_x, \xi_y, \xi_z, t)\mathrm{d}\xi_y. \end{cases} \tag{10}$$

Numerical simulations were performed for the Boltzmann equations for the distribution functions f_{xz} and h_{xz}, and the time development of the macroscopic variables was calculated using the following equations:

$$\rho = \int\int_{-\infty}^{\infty} f_{xz}\mathrm{d}\xi_x\mathrm{d}\xi_z, \quad v_z = \frac{1}{\rho}\int\int_{-\infty}^{\infty} \xi_z f_{xz}\mathrm{d}\xi_x\mathrm{d}\xi_z,$$

$$v_x = \frac{1}{\rho}\int\int_{-\infty}^{\infty} \xi_x f_{xz}\mathrm{d}\xi_x\mathrm{d}\xi_z,$$

$$T = \frac{1}{3\rho R}\left(\int\int_{-\infty}^{\infty}\left[(\xi_x - v_x)^2 + (\xi_z - v_z)^2\right] f_{xz}\mathrm{d}\xi_x\mathrm{d}\xi_z + \int\int_{-\infty}^{\infty} h_{xz}\mathrm{d}\xi_x\mathrm{d}\xi_z\right),$$

where v_x and v_z are the gas velocities for x and z directions and T is the gas temperature. In this study, v_z is almost zero due to the nature of the problem. 300 and 200 grids were utilized for the velocity space ξ_x, ξ_z and physical space z, respectively. Nonuniform and uniform grids were utilized for the velocity and physical spaces, respectively: in the velocity space, the minimum size was $\Delta\xi_z/\sqrt{2RT} = 1.0^{-4}$ near $\xi_z = 0$ and the maximum size was $\Delta\xi_z/\sqrt{2RT} = 1.0^{-2}$ far from $\xi_z = 0$. The same grid size was applied in ξ_x space. Furthermore, for physical space, the grid size in the case of largest system was $\Delta z/\lambda = 6.7 \times 10^{-2}$.

As can be seen from Fig. 2, the gas flow is symmetrical between the upper and lower halves of the system, so we consider the upper half of the system. The following diffuse reflections were used as the boundary conditions for the upper wall boundary of the molecules with $\xi_z < 0$,

$$f_{\mathrm{wall}} = \frac{\rho^*}{(2\pi RT)^{3/2}} \exp\left(-\frac{(\xi_x - V_w)^2 + \xi_y^2 + \xi_z^2}{2RT}\right), \tag{11}$$

where ρ^* is the saturated vapor density at temperature T and V_w is the wall speed ($V_w = 50$ m/s). Diffuse reflections are used as the boundary conditions for the liquid boundary of molecules at the upper liquid surface with $\xi_z > 0$,

$$f_{\mathrm{liquid}} = \frac{\rho^*}{(2\pi RT)^{3/2}} \exp\left(-\frac{\xi_x^2 + \xi_y^2 + \xi_z^2}{2RT}\right). \tag{12}$$

Because each of these boundary conditions is a similar diffuse reflection, the slip velocities at the wall and liquid boundaries are equal resulting in a symmetric flow, where the average velocity is at the center of the flow in the case of Couette flow. If the velocity profile $v_x(z)$ obtained from the MD simulation agrees with that obtained from the simulation above, these boundary conditions, which were isotropic diffuse reflections, can be considered appropriate.

III. RESULTS

A. Couette flow between wall boundaries: Determination of position to impose kinetic boundary condition for wall boundary

First, MD simulations were performed in the absence of a liquid to investigate whether the velocity distribution of the gas molecules on the wall was a diffuse reflection. MD simulations were performed with smooth solid walls at the top and bottom of the system and Ar gas molecules between them, as shown in Fig. 3(a). The wall and Ar gas were equilibrated at 85, 95, and 105 K to obtain the initial conditions. The top wall moved at a velocity of $V_w = 50$ m/s in the positive x-direction, and the bottom wall was assumed to have a velocity of 0 m/s. The number of Ar gas molecules was adjusted to approximately equal the saturated vapor density at each temperature to match the conditions in the calculation with the liquid described below. The saturated vapor density obtained from the MD simulation is about 4.77 kg/m^3 at 85 K, 11.44 kg/m^3 at 95 K, and 24.03 kg/m^3 at 105 K, and these values are consistent with vapor densities from previous studies for each temperature.[13] In addition, we have confirmed that the temperature dependence of the transition layer thickness at the gas–liquid interface is almost consistent with previous studies. The values of $\Xi = p/(\rho RT)$ at various temperatures of argon were shown as $\Xi = 0.98$ at 85 K, $\Xi = 0.95$ at 95 K, and $\Xi = 0.90$ at 105 K (see Ref. 13). As the saturated vapor density increases with temperature, the value of Ξ deviates from 1, but as will be shown later in this MD simulation, the ideal gas approximation is almost valid in this temperature range (see

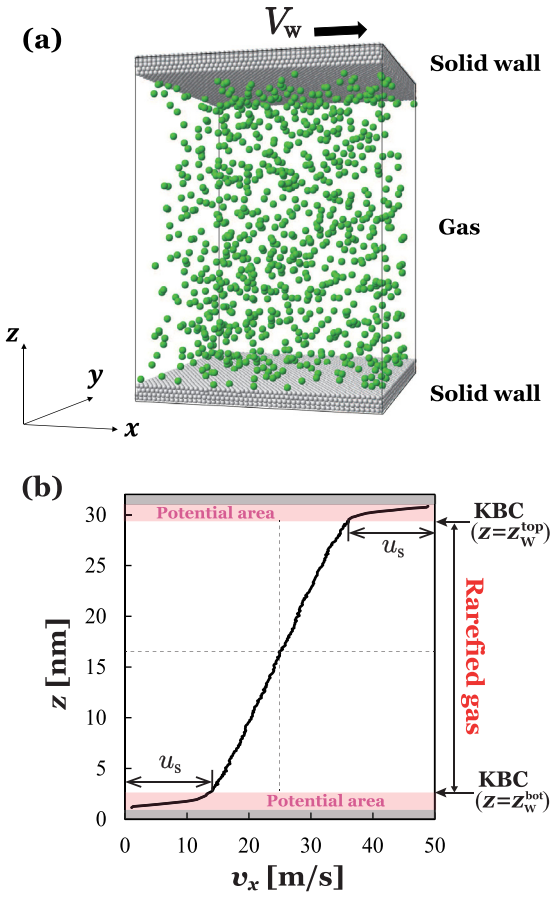

FIG. 3. (a) Snapshot of MD simulation for rarefied gas Couette flow between smooth walls and (b) velocity profile obtained from the MD simulation at 95 K.

the result of Fig. 4). The Knudsen number was varied from 0.2 to 5.9 in the simulations. The Mach number for each temperature was $\mathrm{Ma} = V_w/\sqrt{\gamma RT} = 0.291$ at 85 K, $\mathrm{Ma} = 0.275$ at 95 K, and $\mathrm{Ma} = 0.262$ at 105 K, where $\gamma = 5/3$ is the ratio of specific heats. Although there is some difference in the Mach number, we confirm that this slight difference in the Mach number has no effect on the non-dimensionalized slip velocity using the wall velocity V_w.

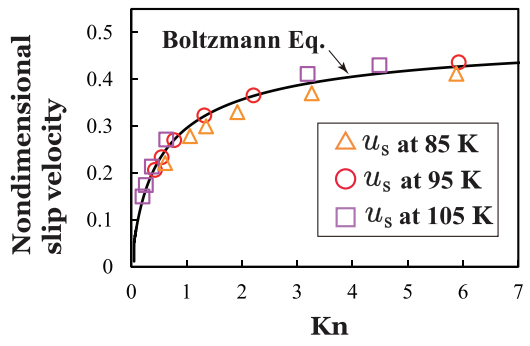

FIG. 4. Relation between slip velocity and Kn number in the case of smooth wall boundaries for each temperature.

Figure 3(b) shows the velocity profile of Ar gas obtained from MD simulations at 95 K, $L_z = 32$ nm, and the gas density 11.44 kg/m^3 as one example. The horizontal axis represents the velocity, and the vertical axis is the z-coordinate. The same wall was used for both the top and bottom walls, with the top wall moving at $V_w = 50$ m/s in the x direction and the bottom wall remaining stationary.

The gray areas with thickness $l = 1.030$ nm from the top and bottom boundaries were solid walls. The pink area represents the area where the influence of the intermolecular forces due to the solid wall is considered non-negligible. The intermolecular forces of the wall molecules were assumed to limit the distance from the wall to ~5.5 times of $\sigma_{\mathrm{Ar-Pt}}$ ($5.5\,\sigma_{\mathrm{Ar-Pt}} = 1.617\,\mathrm{nm} = \ell_w$). This is almost equivalent to the cutoff distance used in MD simulations, and previous studies have treated it similarly.[6] For convenience, this position is denoted as $z = z_w^{top} = L_z - l - \ell_w$ for the top wall and $z = z_w^{bot} = l + \ell_w$ for the bottom wall.

The difference between the velocities of the rarefied gas at $z = z_w^{top}$ and $z = z_w^{bot}$, and those of the walls V_w and 0 are the slip velocities u_s. The velocity profile was 25 m/s $= V_w/2$ at the center of the system. The magnitudes of the top and bottom slip velocities were nearly equal. Since the same wall was used on the upper and lower sides, the velocity distribution was symmetrical on the upper and lower sides.

Figure 4 shows the relationship between the Kn number and slip velocity u_s. The horizontal axis represents the Kn number, and the vertical axis represents the slip velocity non-dimensionalized by the wall velocity. The black lines indicate the slip velocities obtained by solving the Boltzmann equation [Eq. (6)] with the diffuse reflection boundary conditions [Eqs. (11) and (12)]. The markers indicate the slip velocity of the wall boundary in the MD simulations at each temperature. For MD simulations, the mean free path of the gas molecules was estimated using the following equation:

$$\lambda = \frac{1}{\sqrt{2}n\pi\sigma_{\mathrm{Ar}}^2}, \tag{13}$$

where n denotes the number density of the gas molecules. Although there were top and bottom walls in the MD simulation, as mentioned earlier, the slip velocities on both sides of the wall had the same magnitude; therefore, they are shown with a single marker.

All results of the MD simulations agree with the results of the Boltzmann equation at each temperature: at 85 K, the overall slip velocity was slightly lower than that obtained using the Boltzmann equation, and at 105 K, the slip velocity was slightly higher than that obtained using the Boltzmann equation. This is due to the effect of Ar molecules adsorbed on the wall. In these simulations, the density of gas molecules was set to reproduce the saturated vapor density at each temperature. This difference in gas density affected the value of the gas density layer (adsorption layer) on the wall. This difference in the adsorption layers may be the cause of misalignment of the boundary or a slight deviation from perfect diffuse reflection. However, the results are almost consistent with those of the Boltzmann equation, which sets the boundary conditions for diffuse reflection at each temperature. The wall boundary positions ($z = z_w^{top}$ or z_w^{bot}) are

appropriate for the boundary conditions of the Boltzmann equation, and the walls used in this study were considered to be isotropic diffuse reflections.

B. Couette flow between wall and liquid boundaries: Gas velocity profile and slip velocity on liquid boundaries

Next, the velocity profile of Ar vapor molecules sandwiched between the liquid and solid walls, and the slip velocities at the liquid boundary and wall were investigated using the calculation system shown in Fig. 2.

Figure 5(a) shows the velocity profiles of Ar vapor and liquid obtained from MD simulations. A typical velocity profile at 95 K and $L_z = 52$ nm is presented. The horizontal axis represents the velocity, and the vertical axis is the z-coordinate. We introduce a new coordinate system Z. $Z = z - L_z/2 = 0$ is the center of the liquid film, and the gray area is the solid wall. The green area at the bottom indicates the liquid film. The pink areas represent the areas of intermolecular forces created by the liquid film and wall.

The distance affected by intermolecular forces on the liquid side was defined as the distance from the liquid film surface to a position with thrice the thickness of the density transition layer, based on our recent studies.[14–19] The thickness of the transition layer is represented by the approximate curve in Eq. (14) [Fig. 5(b)]. The nonlinear least squares method was used for fitting the density transition layer,

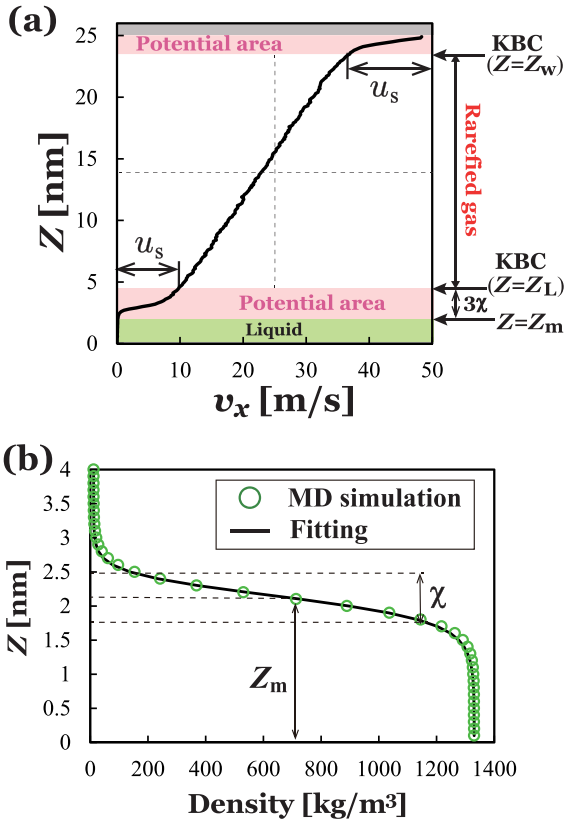

FIG. 5. (a) Velocity profile obtained from the MD simulation at 95 K and (b) density profile at the vapor–liquid interface.

$$\rho(Z) = \frac{\rho_v + \rho_l}{2} + \frac{\rho_v - \rho_l}{2}\tanh\left(\frac{Z - Z_m}{0.455\chi}\right), \tag{14}$$

where ρ_l is the liquid-phase density of Ar and ρ_v is the gas-phase density of Ar. Z_m is the distance from the center of the liquid film to the center of the transition layer, and χ denotes the thickness of the transition layer. Using the obtained Z_m and χ, $Z_L = Z_m + 3\chi$ represents the position at which the intermolecular forces of the liquid film are reached. The difference between the velocities at $Z = Z_L$ and 0 m/s in the liquid film, and the difference between the velocities at $Z = Z_w = L_z/2 - l - \ell_w$ and $V_w = 50$ m/s on the solid wall is slip velocities.

Figure 6 shows the relationship between the Kn number and the slip velocity. The horizontal axis represents the Kn number, and the vertical axis represents the non-dimensionalized slip velocity in terms of the wall velocity. The black line represents the slip velocity obtained by solving the Boltzmann equation [Eq. (6)] with diffuse reflection boundary conditions: [Eqs. (11) and (12)], and the markers represent the slip velocities of the wall and liquid boundaries obtained from the MD simulations.

In the MD simulation, a difference was observed between the slip velocities on the wall and liquid sides, which decreased when Kn is small. When Kn = 0.12, the slip velocities of the wall and the liquid were almost the same, which is consistent with the results of the Boltzmann equation analysis with diffuse boundaries. This implies that the position of the vapor–liquid boundary in the Boltzmann equation is appropriate at $Z = Z_L$.

However, the slip velocity at the wall boundary in the MD simulation was higher than that of the Boltzmann equation analysis and that at the liquid boundary is smaller in the case of a high Kn. Thus, in the MD simulation, the wall side is more slippery than that obtained from the Boltzmann equation, and the liquid side is less slippery. Owing to these differences in slip velocities, the vapor velocities at the center of the liquid and wall do not equal $V_w/2$, resulting in an asymmetric velocity profile [Fig. 5(a)]. The asymmetry of the slip velocity was due to backscattering at the liquid boundary caused by the molecular-scale boundary roughness of the liquid. This is discussed in detail in the Appendix.

C. Modified kinetic boundary condition at liquid boundary

As shown in the Appendix, the velocity slip phenomenon at the liquid boundary was caused by the backscattering of the reflected

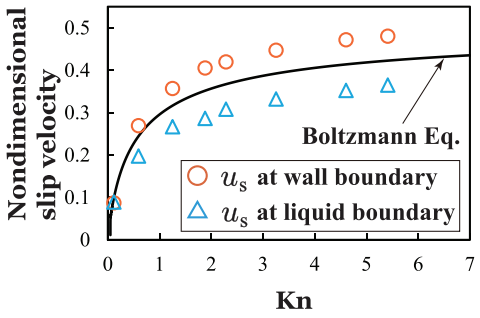

FIG. 6. Relation between slip velocity and Kn number in the case of smooth wall and liquid boundaries in the case of 95 K.

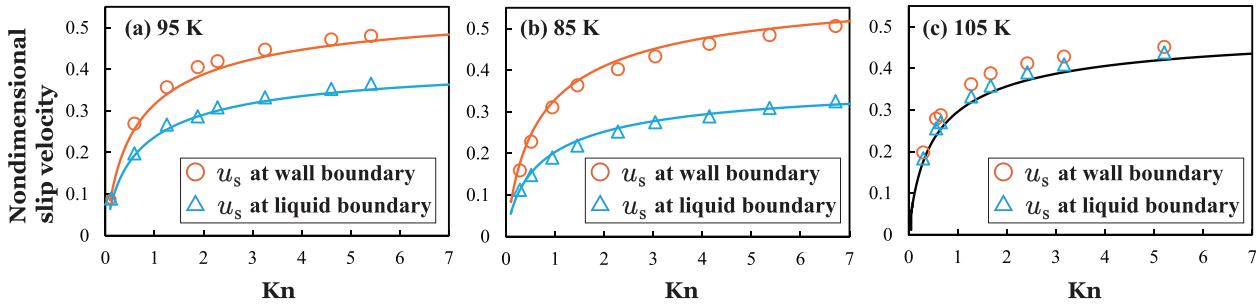

FIG. 7. Relation between slip velocity and Kn number in the case of smooth wall and liquid boundaries for each temperature; (a) 95 K ($\beta = 1.16$), (b) 85 K ($\beta = 1.28$), and (c) 105 K (diffuse reflection).

molecules. In this section, the boundary condition used to describe the backscattering of this gas molecule is introduced, and the Boltzmann equation is analyzed.

For the wall boundary condition, we showed in Sec. III A that diffuse reflection is consistent with the MD simulation results. Therefore, the wall boundary condition is the same as that in Sec. II B, as in Eq. (11). We need to modify the liquid boundary condition to express the backscattering of the reflected molecules. In this study, the modified Maxwell-type boundary condition was used with reference to the previous study:[20]

$$f^{\mathrm{Mod}}_{\mathrm{liquid}}(Z_{\mathrm{L}}, \boldsymbol{\xi}) = \int_{\tilde{\xi}_z<0} \left|\frac{\tilde{\xi}_z}{\xi_z}\right| K_M(\tilde{\boldsymbol{\xi}}, \boldsymbol{\xi}) f(Z_{\mathrm{L}}, \tilde{\boldsymbol{\xi}}) \mathrm{d}\tilde{\boldsymbol{\xi}}, \tag{15}$$

$$K_M(\tilde{\boldsymbol{\xi}}, \boldsymbol{\xi}; \alpha, \beta) = \left[(1-\alpha)\delta(\xi_z + \tilde{\xi}_z) + \alpha \frac{|\xi_z|}{RT} \times \exp\left(-\frac{\xi_z^2}{2RT}\right)\right] \times \left[(\beta - 1)\delta(\xi_x + \tilde{\xi}_x)\delta(\xi_y + \tilde{\xi}_y) + \frac{(2-\beta)}{2\pi RT} \exp\left(-\frac{\xi_x^2 + \xi_y^2}{2RT}\right)\right], \tag{16}$$

where $\tilde{\boldsymbol{\xi}} = (\tilde{\xi}_x, \tilde{\xi}_y, \tilde{\xi}_z)$ is the molecular velocity of an incident molecule from the gas to the liquid phase and $\boldsymbol{\xi} = (\xi_x, \xi_y, \xi_z)$ denotes the molecular velocity of the reflected molecule at the boundary. The main parameters in Eq. (16) are α and β. α is the energy accommodation coefficient that represents the normal-direction component of the reflected molecules at the boundary and is between 0 and 1. Here, α was always set to 1. β is the tangential momentum accommodation coefficient (TMAC), which represents the tangential component of the reflected molecules to the boundary and should be greater than 1 and less than or equal to 2. Setting the parameters $\alpha = 1$ and $\beta \to 1$ yields under the boundary conditions of a perfect diffuse reflection [Eq. (12)]. The larger the value of β, the greater the effect of backscattering.

Figure 7(a) shows the relationship between the Kn number and slip velocity in the Boltzmann equation with modified boundary conditions for the liquid side [Eq. (15)] and boundary conditions [Eq. (11)] on the walls at 95 K. In this case, we used $\beta = 1.16$. The horizontal axis represents the Kn number, and the vertical axis is the nondimensionalized slip velocity in terms of the wall velocity. The solid orange line shows the slip velocity on the wall, and the solid light blue line indicates the slip velocity on the liquid side. The orange markers indicate the slip velocity on the wall side of the MD simulation, and the light blue markers indicate the slip velocity on the liquid side. These results of the Boltzmann equation analysis are in good agreement with the MD simulation results for $\beta = 1.16$ at 95 K. The results showed that the difference between the slip velocity of the liquid boundary and that of the wall can be described by a boundary condition that incorporates backscattering.

Figures 7(b) and 7(c) show the results for the 85 and 105 K cases. The black lines in Fig. 7(c) show the slip velocity obtained by solving the Boltzmann equation with the boundary condition of perfect diffuse reflection [Eq. (12)] for a liquid boundary. First, the results for 85 K show that the difference in slip velocity between the wall and liquid boundary is larger than that at 95 K. This is due to the fact that the liquid boundary is more slippery at 85 K than the case of 95 K. If the value of the coefficient β of the modified boundary condition is set to 1.28, the results of the MD simulation and the Boltzmann equation are in agreement. However, the results at 105 K show that the difference between the slip velocities of the wall and liquid boundary is smaller and has almost the same values. Thus, the value of β is very close to 1, indicating that the trend is almost the same as that of a perfect diffuse reflection.

Here, we consider the local Knudsen number near the liquid boundary at each temperature. The representative length is the thickness of the potential area near the liquid boundary [Fig. 5(a)], which is three times the thickness of the transition layer χ at each temperature:

$$\mathrm{Kn}_{\mathrm{local}} = \frac{\lambda}{3\chi}. \tag{17}$$

The $\mathrm{Kn}_{\mathrm{local}}$ values for each temperature are listed in Table I. At 85 K, $\mathrm{Kn}_{\mathrm{local}}$ was relatively large, indicating that the collisions between vapor molecules are small in the vicinity of the liquid boundary. However, at 105 K, $\mathrm{Kn}_{\mathrm{local}}$ was relatively small, indicating an increase in collisions between vapor molecules compared with lower temperatures. The collision between vapor molecules changes the velocity distribution function of the molecules exiting the liquid phase to the gas phase from

TABLE I. Local Knudsen number for each temperature conditions.

T (K)	χ (nm)	$\mathrm{Kn}_{\mathrm{local}}$
85	0.668	13.5
95	0.787	4.66
105	0.932	1.90

anisotropic to isotropic. The molecular collisions between vapor molecules on the boundary increased with increasing temperature. This may be one reason for approaching perfect diffuse reflection at high temperatures.

IV. CONCLUSION

In this study, molecular dynamics simulations were performed for the Couette flow of a rarefied gas between a liquid and a wall. These results were further discussed in context of the Boltzmann equation analysis, particularly with respect to the gas–liquid boundary conditions. The following findings were obtained:

(i) The slip velocity on the liquid boundary was smaller and that on the solid boundary was larger, resulting in an asymmetric velocity field of Couette flow as the Kn number increases.
(ii) For the results obtained in (i), the Boltzmann equation analysis was performed using boundary conditions that consider backscattering. It was confirmed that the slip velocity asymmetry could be determined.
(iii) The difference between the slip velocities at the wall and liquid boundaries decreases as the system temperature increases. One of the reasons for this is related to the collisions between vapor molecules near the liquid boundary.

ACKNOWLEDGMENTS

This study was supported by JST, PRESTO Grant No. JPMJPR21O3, Japan to K.K.

AUTHOR DECLARATIONS

Conflict of Interest

The authors have no conflicts to disclose.

Author Contributions

Kazumichi Kobayashi: Conceptualization (lead); Data curation (equal); Formal analysis (equal); Funding acquisition (equal); Investigation (equal); Methodology (equal); Project administration (lead); Resources (equal); Supervision (equal); Writing – original draft (equal); Writing – review & editing (lead). **Kota Aoki:** Data curation (lead); Formal analysis (equal); Investigation (equal); Methodology (equal); Software (equal); Visualization (lead); Writing – review & editing (supporting). **Hirofumi Tabe:** Investigation (equal); Software (lead); Writing – review & editing (equal). **Hiroyuki Fujii:** Conceptualization (supporting); Writing – review & editing (equal). **Toshiki Nara:** Software (supporting); Writing – review & editing (supporting). **Hideyoshi Takashima:** Software (supporting); Writing – review & editing (supporting). **Nobuyuki Oshima:** Software (supporting); Writing – review & editing (supporting). **Masao Watanabe:** Conceptualization (supporting); Writing – review & editing (equal).

DATA AVAILABILITY

The data that support the findings of this study are available from the corresponding author upon reasonable request.

APPENDIX: BACKSCATTERING OF GAS MOLECULES AT ROUGH WALL SURFACE

In the MD simulation, the phenomenon in which the gas flow is more slippery on the wall side than the result obtained from the Boltzmann equation and less slippery on the liquid boundary side is described in Sec. III B. It was assumed that this was due to the backscattering of gas molecules caused by molecular-level capillary waves disturbing the liquid boundary rather than the wall boundary. Therefore, as illustrated in Fig. 8(a), a solid wall with a smooth boundary was placed at the top of the system, and a solid wall with a rough boundary and uneven surface of one platinum molecule was placed at the bottom of the system, as shown in Fig. 8(b). Ar gas molecules were placed between the smooth and rough walls. The top wall was moved at a velocity of 50 m/s in the positive x direction, and the bottom wall was assumed to have a velocity of 0. As shown in Fig. 8(b), the rows of Pt molecules were arranged such that they are perpendicular to the direction of movement of the top wall, representing the unevenness of the molecular scale. The gas density was adjusted to the saturated vapor density at 95 K (11.44 kg/m^3) to match the conditions of the system described previously.

Figure 9 shows the relationship between the Knudsen number and slip velocities at the top and bottom walls. As shown in the figure, the slip velocity is different at the top smooth and lower rough boundaries. It can also be observed that the top boundary is more slippery, and the lower boundary is less slippery, similar to the liquid case. This result is similar to those for the liquid and smooth-wall conditions, as shown in Fig. 6. Hence, this indicates that the roughness caused by molecular-scale fluctuations on the boundary

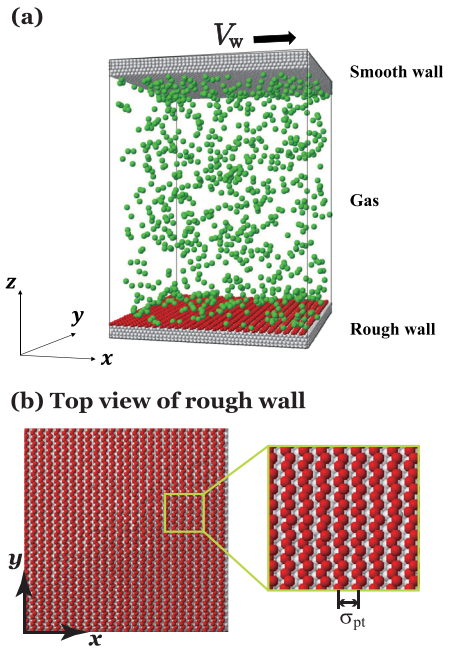

FIG. 8. (a) Snapshot of MD simulation for rarefied gas Couette flow between smooth and rough walls and (b) top view of rough wall boundary.

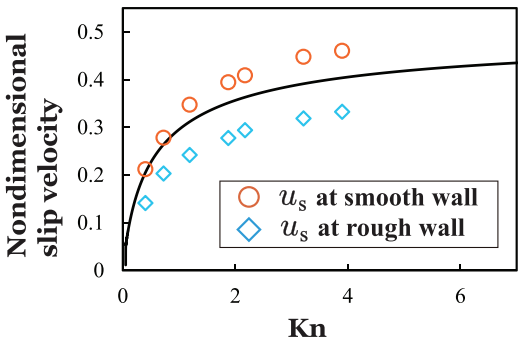

FIG. 9. Relation between slip velocity and Kn number in the case of smooth and rough wall boundaries.

causes backscattering of molecules, which leads to a lower slip velocity.

REFERENCES

[1]M. V. Chubynsky, K. I. Belousov, D. A. Lockerby, and J. E. Sprittles, "Bouncing off the walls: The influence of gas-kinetic and van der Waals effects in drop impact," Phys. Rev. Lett. **124**, 084501 (2020).

[2]P.-G. de Gennes, "On fluid/wall slippage," Langmuir **18**, 3413–3414 (2002).

[3]K. Yamamoto, H. Takeuchi, and T. Hyakutake, "Characteristics of reflected gas molecules at a solid surface," Phys. Fluids **18**, 046103 (2006).

[4]K. Yamamoto, H. Takeuchi, and T. Hyakutake, "Scattering properties and scattering kernel based on the molecular dynamics analysis of gas-wall interaction," Phys. Fluids **19**, 087102 (2007).

[5]H. Yamaguchi, Y. Matsuda, and T. Niimi, "Molecular-dynamics study on characteristics of energy and tangential momentum accommodation coefficients," Phys. Rev. E **96**, 013116 (2017).

[6]M. Barisik and A. Beskok, "Scale effects in gas nano flows," Phys. Fluids **26**, 052003 (2014).

[7]S. W. Sides, G. S. Grest, and M.-D. Lacasse, "Capillary waves at liquid-vapor interfaces: A molecular dynamics simulation," Phys. Rev. E **60**, 6708 (1999).

[8]M. Kon, K. Kobayashi, and M. Watanabe, "Method of determining kinetic boundary conditions in net evaporation/condensation," Phys. Fluids **26**, 072003 (2014).

[9]H. Tabe, K. Kobayashi, H. Yaguchi, H. Fujii, and M. Watanabe, "Influence of liquid–solid intermolecular force on levitation of impacting nanodroplet," Heat Mass Transfer **55**, 993–1003 (2019).

[10]H. Tabe, K. Kobayashi, H. Yaguchi, H. Fujii, and M. Watanabe, "Levitation mechanism of impacting nanodroplet on heated wall," Int. J. Therm. Sci. **150**, 106203 (2020).

[11]P. Andries, P. Le Tallec, J.-P. Perlat, and B. Perthame, "The Gaussian-BGK model of Boltzmann equation with small Prandtl number," Eur. J. Mech. - B/Fluids **19**, 813–830 (2000).

[12]C. Chu, "Kinetic-theoretic description of shock wave formation. II," Phys. Fluids **8**, 1450–1455 (1965).

[13]S. Fujikawa, T. Yano, and M. Watanabe, *Vapor-Liquid Interfaces, Bubbles and Droplets: Fundamentals and Applications* (Springer Science & Business Media, 2011).

[14]K. Ohashi, K. Kobayashi, H. Fujii, and M. Watanabe, "Evaporation coefficient and condensation coefficient of vapor under high gas pressure conditions," Sci. Rep. **10**, 8143 (2020).

[15]H. Tabe, K. Kobayashi, H. Fujii, and M. Watanabe, "Molecular dynamics study on characteristics of reflection and condensation molecules at vapor–liquid equilibrium state," PLoS One **16**, e0248660 (2021).

[16]K. Ohashi, K. Kobayashi, H. Fujii, and M. Watanabe, "Mean-field kinetic theory analysis of vapor flow between evaporating and condensing interfaces in the presence of non-condensable gas molecules," Phys. Fluids **33**, 122017 (2021).

[17]H. Tabe, K. Kobayashi, H. Fujii, and M. Watanabe, "Molecular dynamics simulation of evaporation coefficient of vapor molecules during steady net evaporation in binary mixture system," Int. J. Heat Mass Transfer **188**, 122663 (2022).

[18]H. Tabe, K. Hiramatsu, K. Kobayashi, H. Fujii, M. Watanabe, and T. Totani, "Molecular dynamics study of evaporation induced by locally heated argon liquid," Appl. Therm. Eng. **212**, 118472 (2022).

[19]K. Ohashi, K. Kobayashi, H. Fujii, and M. Watanabe, "Vapor condensation induced by fast-moving liquid film in the presence of noncondensable gas molecules," Int. Commun. Heat Mass Transfer **142**, 106622 (2023).

[20]S. Kosuge, "Cylindrical Couette flow of a rarefied gas: Effect of a boundary condition on the inverted velocity profile," Phys. Rev. E **92**, 013013 (2015).